Electro-Optic Near-Field Mapping of Planar Resonators

Torsten Pfeifer, Torsten Löffler, Hartmut G. Roskos, Heinrich Kurz, Markus Singer, and Erwin M. Biebl

***Abstract*—A comprehensive experimental and theoretical study for the determination of the electric near-field above planar resonators is presented. The transverse component of the electric field is mapped by external electro-optic (EO) sampling technique with high spatial and temporal resolution. The evolution of the near-field radiation pattern of the investigated 7-GHz planar resonator to the onset of the far-field pattern is traced by measurements at various heights above the sample. Frequency-dependent measurements allow to characterize the field pattern changes when the frequency is swept through the main resonance. Additional undesired resonances are identified by the detected mode pattern. The experimental data are reproduced by simulations based upon an electric field integral equation (EFIE) method.**

***Index Terms*—Electro-optic measurements, resonators.**

I. Introduction

PLANAR radiating resonators have gained increasing interest for receiving and transmitting applications in the millimeter-wave region. Particular advantages are the capability of very easy monolithic integration of a complete radiating oscillator, a high degree of technological reproducibility, small size, and, thus, low cost. The design of such oscillators must avoid excitation of parasitic surface waves or undesired patch or microstrip modes resulting in a reduced Q-factor, additional instability, and a distorted radiation pattern at the desired operation frequency. Usually, experimental characterizations of oscillators radiating at millimeter-wave frequencies cover the *far* field. The data allow to identify faulty operation of the device, but it is often difficult to determine the origin of the malfunction. During the design phase of transmitters, ponderous model calculations are required to track down errors in the layout. A much more direct experimental tool for error identification is measurements in the *near* field of planar radiators. They give detailed information about the spatial characteristics of the electric field distribution. Parts of the structure that cause parasitic resonances, e.g., bias lines, are identified easily by the detected mode pattern.

In this paper, the electric near field (amplitude and phase) of a planar 7-GHz resonator is mapped by external electro-optic (EO) detection employing a novel femtosecond-laser synchronization scheme [1], [2]. This technique enables mapping of the radiation pattern above the device under test with a μm spatial resolution and a high bandwidth of at least 150 GHz. Earlier EO measurements have employed the internal EO effect of the substrate material to map field distributions within the substrate under the circuit. A great advantage of EO external detection compared to the established internal EO sampling technique [3]–[5] is its independence of the substrate material. In addition, in the case of internal EO mapping, the substrate must be optically accessible. Parts of the circuit, which are covered by opaque layers on both sides of the substrate are excluded from the measurement, e.g., the field distribution of antennas with backside metallization is not detectable on the complete structure. External EO sampling overcomes this limitation. Additionally, it provides the capability of measuring the free-space radiation pattern for various distances from the sample [6]–[8] instead of averaging over the distance (substrate thickness) as for internal sampling.

First, the theory necessary for the calculation of the electric near field above planar resonators is developed. The setup of the EO field mapping system as well as the design and the fabrication of the investigated planar 7-GHz resonator are presented in the following sections. A detailed experimental and theoretical study of the transverse electric near-field distribution of the 7-GHz resonator is performed. Amplitude and phase of the transverse electric field are mapped simultaneously for varying oscillation frequencies tuned through the resonance at different testing heights. Elements of the resonators responsible for the excitation of parasitic microstrip and patch modes are clearly identified.

II. Theory

The field theoretical problem for the calculation of the tangential electric near field above a planar circuit is shown in Fig. 1. In our case, we restrict the theory to planar resonators with in-plane excitation without z components. The structure consists of a layered medium. On top of layer one, a planar resonator A' with arbitrary shape is located. The lossy metallization with the surface resistance Z_s is thin compared to an electrical wavelength. The substrate of layer one is also lossy (ε_1, μ_1, $\tan\delta_1$), metallized on the backside (Z_s) of thickness h_1, and assumed to extend infinitely. Layer two is of thickness h_2 and filled with air (ε_0, μ_0). The measurement plane is on the top of layer two. Above layer two we assume free-space. A

Manuscript received August 2, 1996; revised February 24, 1997. This work was supported by the BMBF under Contract 01 M 2938 B.

T. Pfeifer, T. Löffler, H. G. Roskos, and H. Kurz are with the Institut für Halbleitertechnik II, Rheinisch-Westfälische Technische Hochschule Aachen, Aachen, D-52056 Germany.

M. Singer and E. M. Biebl are with the Lehrstuhl für Hochfrequenztechnik, Technische Universität München, München, D-80333 Germany.

Publisher Item Identifier S 0018-926X(98)01437-9.

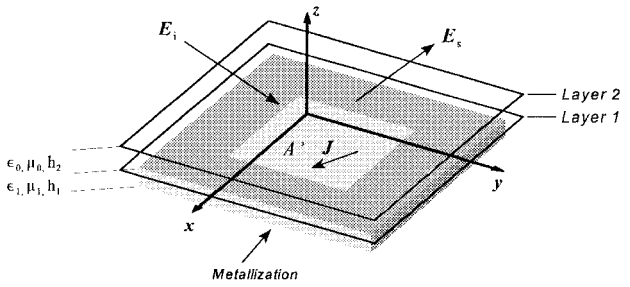

Fig. 1. Scattering in layered media.

rigorous full wave analysis based on the method of moments (MoM) employing Galerkin's method in the spectral domain is used to derive the electric near field above the device under test [9].

In the first step of the analysis, the resulting surface current distribution $\boldsymbol{J}_A$ on the resonator for an incident electric field $\boldsymbol{E}_i^{(1)}$ on layer one is calculated. Owing to the assumption of a planar excitation, $\boldsymbol{E}_i$ consists only of lateral components located in the x-y plane. The electric field integral equation (EFIE) is obtained using the tangential boundary condition of the electric field

$$\begin{aligned}\boldsymbol{e}_z \times \boldsymbol{E}^{(1)}(\boldsymbol{x}) &= \boldsymbol{e}_z \times [\boldsymbol{E}_i^{(1)}(\boldsymbol{x}) + \boldsymbol{E}_s^{(1)}(\boldsymbol{x})] \\ &= Z_s \boldsymbol{e}_z \times \boldsymbol{J}_A(\boldsymbol{x}). \end{aligned} \tag{1}$$

The scattered tangential electric field $\boldsymbol{E}_s$ in layer one is given by an integral of the product of the current distribution $\boldsymbol{J}_A$ with the dyadic electric Green's function $\overline{\overline{G}}^{E(1|1)}$. The superscript $(1|1)$ denotes that the current distribution $\boldsymbol{J}_A$ and the scattered electric field $\boldsymbol{E}_s^{(1)}$ are located on the top of layer one. The resulting EFIE for layer one is given in spectral domain by

$$\begin{aligned}-\boldsymbol{E}_i^{(1)}(\boldsymbol{x}) = \frac{1}{4\pi^2} \iint_{-\infty}^{+\infty} &\left[\overline{\overline{\tilde{G}}}^{E(1|1)}(k_x, k_y, z) - Z_s\right] \\ &\times \tilde{\boldsymbol{J}}_A(k_x, k_y) e^{-j(k_x x + k_y y)}\, dk_x dk_y \end{aligned} \tag{2}$$

where the tilde indicates the spectral representation. This integral equation is solved by means of the MoM, resulting in the linear equation system

$$\boldsymbol{E}^{(1)} = \boldsymbol{Z}^{(1|1)} \cdot \boldsymbol{J}. \tag{3}$$

The elements of $Z^{(1|1)}$ are given in spectral domain by reaction integrals

$$\begin{aligned}Z_{\xi\eta lk}^{(1|1)} = \frac{1}{4\pi^2} \iint_{-\infty}^{+\infty} &\tilde{t}_{\xi l}^{*(1)}(k_x, k_y) \\ &\times \tilde{G}_{\xi\eta}^{E(1|1)}(k_x, k_y) \tilde{b}_{\eta k}^{(1)}(k_x, k_y)\, dk_x dk_y, \\ &\text{with } \xi = x, y \quad \eta = x, y \end{aligned} \tag{4}$$

where t_{xl}, t_{yl}, and b_{xk}, b_{yk} represent the x- and y-oriented testing and basis functions, respectively. The asterisk designates the complex conjugate. The spectral domain dyadic Green's function of the layered medium can be calculated using the immitance approach [16]. The current distribution on the planar resonator is discretized using uniform roof-top basis functions which are defined on square spaced subdomains

$$b_x(x, y) = \begin{cases} \dfrac{1}{D^2}\left(1 - \dfrac{|x|}{D}\right), & |x| < D,\ |y| < \dfrac{D}{2} \\ 0, & \text{otherwise} \end{cases} \tag{5}$$

$$\tilde{b}_x(k_x, k_y) = \frac{\sin^2\left(\dfrac{k_x D}{2}\right)}{\left(\dfrac{k_x D}{2}\right)^2} \cdot \frac{\sin\left(\dfrac{k_y D}{2}\right)}{\left(\dfrac{k_y D}{2}\right)} \tag{6}$$

and similarly for the y orientation. The resonator is excited by a voltage gap on the planar structure. Thus, all elements of the excitation vector $\boldsymbol{E}^{(1)}$ are zero except the one corresponding to the voltage gap. Solving (3) with the straightforward conjugate gradient method the current distribution $\boldsymbol{J}_A$ is determined.

In the next step, the EFIE for the tangential electric field above the planar structure is formulated. The tangential electric field consists only of the scattered field

$$\boldsymbol{E}^{(2)}(\boldsymbol{x}) = \boldsymbol{E}_s^{(2)}(\boldsymbol{x}). \tag{7}$$

As before, $\boldsymbol{E}_s^{(2)}$ is expressed as an integral equation of the current distribution $\boldsymbol{J}_A$ on layer one and a Green's dyad

$$\begin{aligned}\boldsymbol{E}^{(2)}(\boldsymbol{x}) = \frac{1}{4\pi^2} \iint_{-\infty}^{+\infty} &\overline{\overline{\tilde{G}}}^{E(2|1)}(k_x, k_y, z) \\ &\times \tilde{\boldsymbol{J}}_A(k_x, k_y) e^{-j(k_x x + k_y y)}\, dk_x\, dk_y. \end{aligned} \tag{8}$$

Applying the MoM algorithm to (8), the generalized impedance matrix for the mutual coupling between layer one and layer two is obtained

$$\boldsymbol{E}^{(2)} = \boldsymbol{Z}^{(2|1)} \cdot \boldsymbol{J}. \tag{9}$$

With the current distribution in layer one [compare (3)], the tangential electric field above the planar circuit can now be calculated by a single-vector matrix multiplication.

III. Electro-Optic Measurement System

The electric near field above planar devices on arbitrary substrates is measured by external EO sampling technique employing a passively mode-locked Ti : Sapphire laser [2]. The measurement setup is sketched in Fig. 2. The laser produces optical pulses of 150-fs duration at 740-nm wavelength. A higher harmonic of the laser repetition frequency is locked to the frequency to the HF synthesizer by an active control of the laser cavity length [1], [2]. The laser beam is split into two parts. One part is focused into a photoconductive reference detector (PC switch) to generate an electrical signal in the kilohertz range that is employed 1) for stable synchronization between the HF synthesizer [which feeds the device under test (DUT)] and the laser, and 2) to trigger the detection electronics (lock-in amplifier). The second beam is focused into a commercially available $LiTaO_3$ EO transducer [12] for detection of the electric fields above the antenna under test.

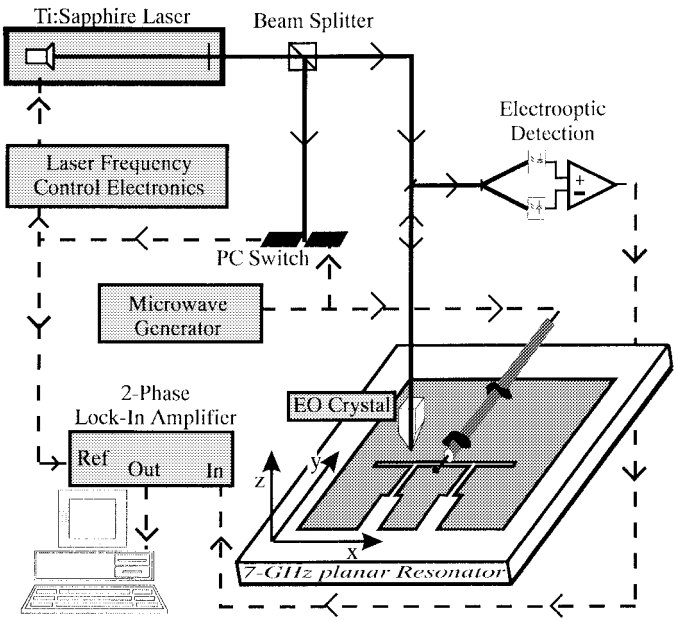

Fig. 2. Schematic of the experimental setup for external electro-optic mapping of electric near-fields above planar resonators. The Ti : Sapphire laser is synchronized to the microwave synthesizer by an active control of the laser repetition frequency. The optical paths and electric paths are indicated by solid and dashed lines, respectively.

The resonator is mounted on a motor-driven x-y-z translation stage and is moved below the EO detector. Magnitude and phase of the electric field above the resonator are analyzed simultaneously with a standard EO differential detection scheme [13] and recorded by a two-phase lock-in amplifier as a function of the spatial coordinates. The spatial resolution of our field-mapping system in x-y direction is limited by the diameter of the laser focus of 10 μm. Due to the millimeter dimensions of our resonator (see the next section), this spatial resolution is sufficient and no efforts have been made to push the spatial resolution to the optical diffraction limit (≤ 1 μm). In z direction, the spatial resolution is determined by the thickness of the EO crystal (20 μm). The resonator frequencies that can be covered are determined by the millimeter-wave source, the laser pulse width, the detector bandwidth, and the timing and frequency jitter of the synchronization [1], [2]. We have demonstrated experimentally frequency locking up to 75 GHz (upper frequency limit of our millimeter-wave source) and an outstanding detection bandwidth of at least 150 GHz superior to field mapping systems based on diode lasers [6] or Nd–YAG lasers [4], [5]. Lock-In detection at 80-kHz reference frequency ensures a high sensitivity of the test system of 1 V/cm [14].

IV. Resonator Design and Fabrication

The layout of our resonator is similar to a design in Si-based millimeter-wave integrated circuit (SIMMWIC) technology for short-range automotive radar applications in the 76 and 93 GHz range [10], [11]. Our structure is a scaled-down model designed for a resonance frequency at 6.7 GHz. A schematic of the resonator is included in Fig. 2. The device employs a 17-μm-thick Cu metallization (grey color) on both sides

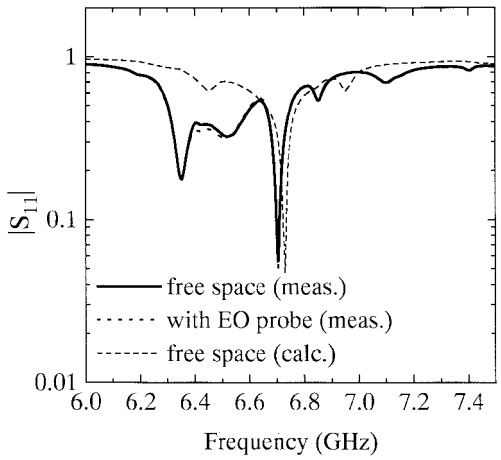

Fig. 3. Magnitude of the S_{11} parameter of the planar resonator. Solid line: S_{11} measured for free-space radiation without EO probe; dotted line: S_{11} measured for free-space radiation with the EO probe positioned at a distance of 50 μm above the slot; dashed line: calculated S_{11} (without EO probe).

of a 1.52-mm-thick Rogers TMM-10 substrate (white color) with a dielectric constant of 9.2. The upper metallization has a 25.25-mm-long and 1.3-mm-wide slot that defines the desired resonance frequency. Gaps are introduced into the metallization at a quarter of the slot length. In the 76-GHz device, the oscillator segments defined by the gaps serve to bias the IMPATT diode located in the center of the slot. In our case, a synthesizer generates the HF signal and feeds the resonator via a semirigid cable connected to the center of the slot. The inner conductor of the cable is soldered to the T-shaped metallization between the gaps. The outer conductor contacts the metal on the other side of the slot.

V. Results

A. Electrical Characterization

The fundamental resonance of our planar resonator is determined by S-parameter measurements with a HP 8510 network analyzer. A one-port open short-match calibration routine for enhanced accuracy is employed. In Fig. 3, the magnitude of the reflection coefficient S_{11} is depicted over a frequency range from 6 to 7.5 GHz. The resonator reveals a main resonance at 6.7 GHz accompanied by weaker and broader resonances at 6.35, 6.55, 6.85, 7.1, and 7.4 GHz. The additional resonances are unwanted and are likely to be introduced by the specific resonator design. For comparison, the calculated reflection coefficient is depicted in Fig. 3. We find a reasonable agreement between the theoretical and experimental curves. The differences of both curves with respect to the frequency and the magnitude of the individual resonances are most likely a result of the laterally finite dimensions of the resonator, the probe station, the position of the clamps for mounting the device, and the semi-rigid cable. All those features have been not considered in the calculations. The identification of parts of the structure, which are responsible for the parasitic resonances, will be investigated with the help of EO field mapping (next section).

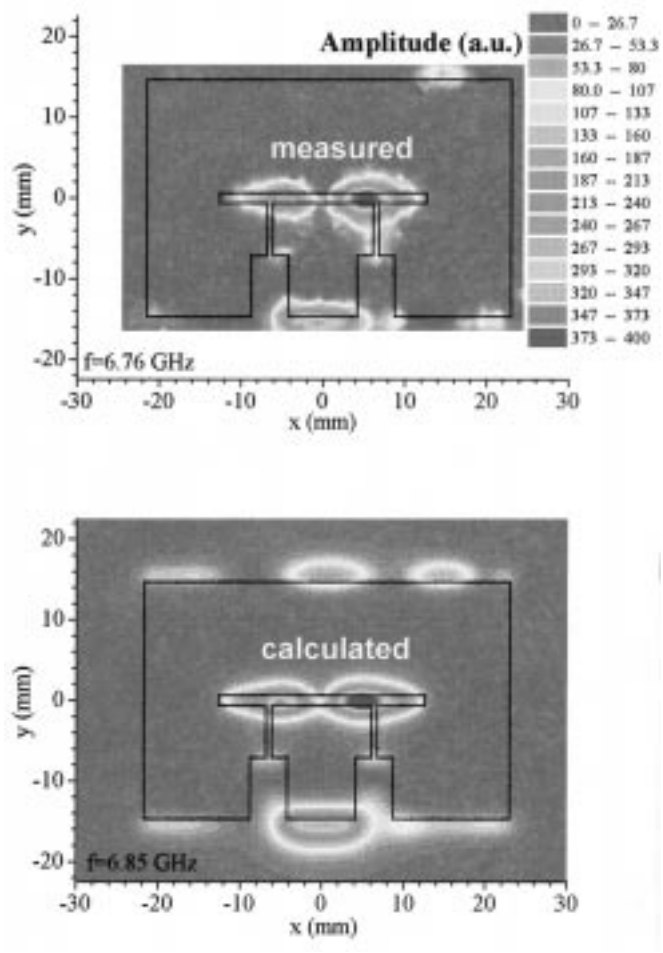

Fig. 4. Measured and calculated amplitude of the y component of the electric field at 6.76 GHz and 1250 μm height. The outline of the frontside metallization is indicated by solid lines.

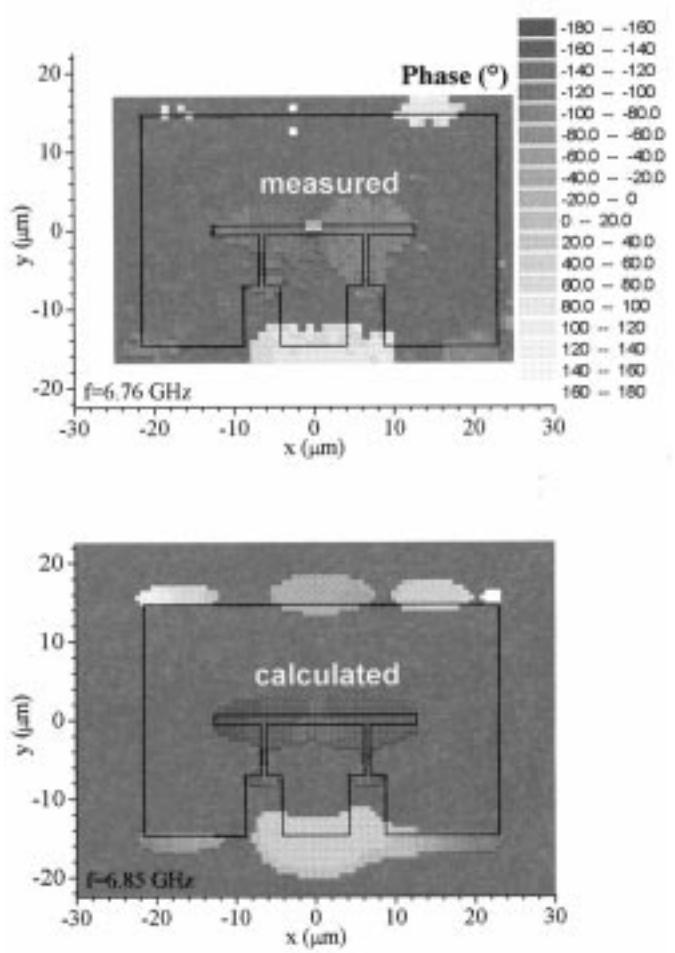

Fig. 5. Measured and calculated phase of the y component of the electric field at 6.76-GHz and 1250-μm height. The outline of the frontside metallization is indicated by solid lines.

A fundamental concern with external near-field testers is the disturbance of the operation of the device under test introduced by the EO probe tip itself. For internal node probing on millimeter integrated circuits (MMIC's), distances $\geq$5–10 μm between the EO probe and the circuit have been reported to be sufficient for noninvasive characterization [15]. However, resonator structures react more sensitively to environmental changes. For this reason, we have experimentally studied the disturbance of our resonator structure introduced by the dielectric nature of the EO detector with 200 $\times$ 200 μm footprint area. The EO probe has been positioned above the resonator and S_{11} has been measured for various detector distances and various positions. No detectable changes in S_{11} have been observed for probe distances of more than 100 μm above the resonator. Only a slight modification of S_{11} around 6.4 GHz is obtained for a distance of 50 μm. In this case, the strongest influence is found when the EO detector is positioned directly above the slot (see dotted line in Fig. 3). From these data, we conclude that the dielectric invasiveness of the EO probe is negligible in the following EO measurements.

B. Optical Characterization

In the upper part of Fig. 4, the measured amplitude of the y component of the transverse electric field above the planar resonator is depicted for a frequency of 6.76 GHz. The amplitude data have been sampled simultaneously with the phase distribution (see Fig. 5) within 30 min (20 dBm input power at the synthesizer). The detection height of 1250 μm (distance from the front face of the resonator to the EO detector) ensures that the EO detector does not collide with the semirigid cable and that the electric near field above the complete resonator is obtained within a single measurement. The signal level scales from red (no signal) to green (medium signal) to blue (strong signal). The fundamental slot mode is detected in the center of the structure. In addition, significant signal contributions are observed at the periphery of the metallization indicating a strong excitation of microstrip-like patch modes. The field distribution is slightly asymmetric about the y axis. This is a result of an asymmetry of the metallization unintentionally introduced in the fabrication process: the right edge of the metallization exceeds the left side by 1.5 mm. All other dimensions are symmetric about the y axis. Evaluation of the phase data (shown in the upper part of Fig. 5) reveal that the signals peaking within the slot and around $x = \pm 20$ mm/$y = -15$ mm are in phase (blue color). All other signals appear with a phase offset of 180° (grey color). This phase distribution can be clearly related to the geometry and temporal

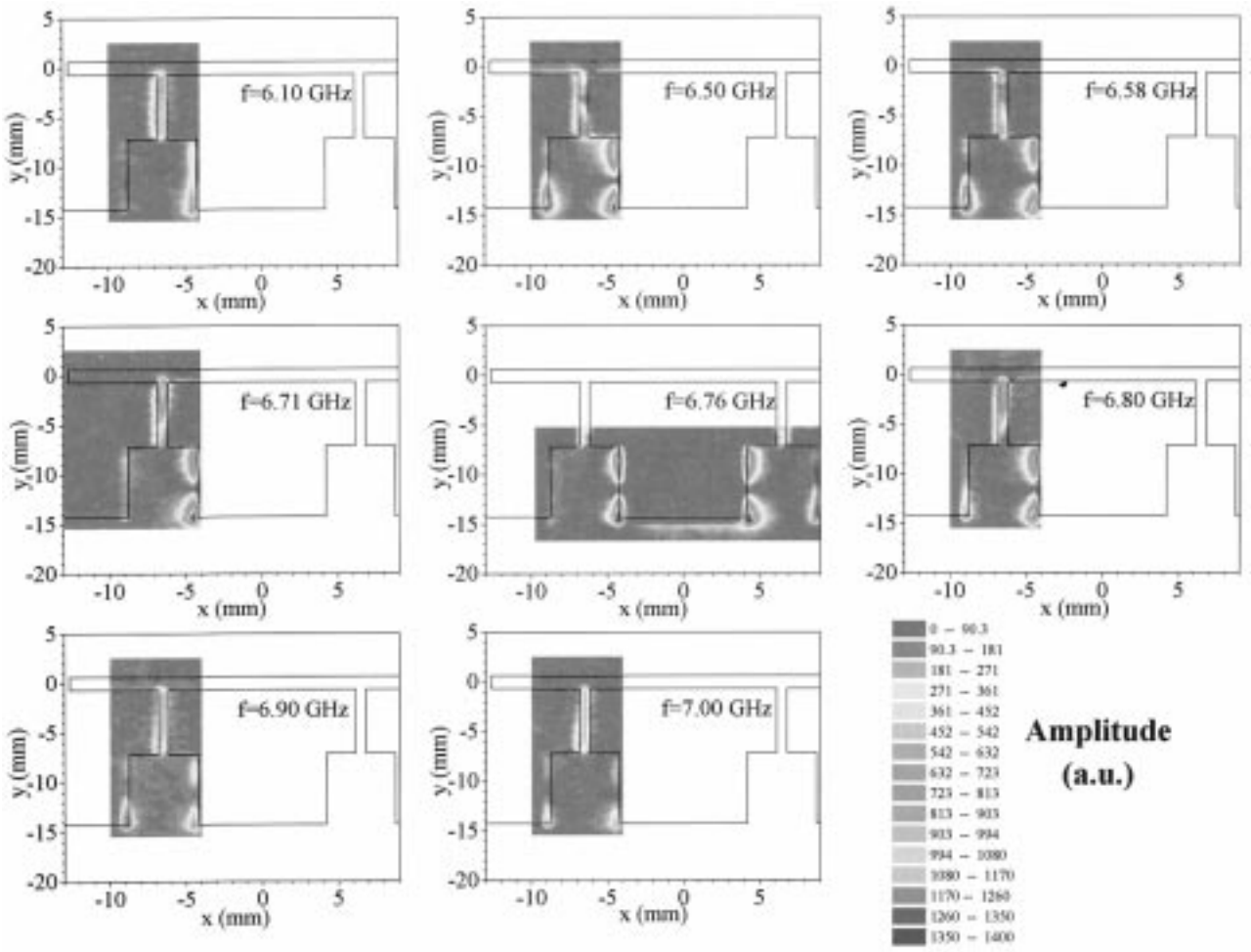

Fig. 6. Magnitude of the x component of the electric field at 50-μm height measured for varying frequencies as indicated in the figure.

dynamics of the electric fields on the resonating structure. Parasitic microstrip-like modes with electric fields from the frontside metallization to the backside metallization are visible at the periphery of the large conductor and the lower part of the T-shaped conductor. The relative phase offset of 180° between the signal contributions at the upper and lower periphery of the large conductor does not indicate an out-of-phase oscillation but is a consequence of the sign reversal of the electric field vector due to the change of conductor alignment. In contrast to these modes, the phase offset between the signals at $x = \pm 20$ mm/$y = -15$ mm and $x = 0$ mm/$y = -15$ mm cannot be explained simply by the conductor configuration, but rather reflects directly the temporal dynamics of the electric fields. The T-shaped conductor and the outer conductor oscillate with a relative phase offset.

The lower parts of Figs. 4 and 5 show results of a model calculation for amplitude and phase of the y component of the electric fields at height 1250 μm and frequency 6.85 GHz. The analysis is based upon the EFIE approach (as explained in Section I) and takes into account ohmic, dielectric, magnetic, and radiation losses, as well as the asymmetry of the resonator. In the calculation, the driving electric field is given by the voltage across the slot in the center of the resonator. The current distribution on the planar slot resonator has been discretized using 5621 uniform roof-top basis functions. The subdomain size D is about 0.647 mm, which is 1/69 of the free-space wavelength at 6.7 GHz. The electric field above the slot resonator is discretized with 15 175 basis functions. On an *HP Series 700* workstation, the calculation of the reaction integrals of $\boldsymbol{Z}^{(1|1)}$ takes 5 h per frequency (hpf). Equation (3) for the determination of the current distribution $\boldsymbol{J}_A$ is solved within further 3 hpf. In addition, the time needed for the calculation of the coupling matrix $\boldsymbol{Z}^{(2|1)}$ and the electric field in layer two $\boldsymbol{E}^{(2)}$ is 8 hpf. Thus, the total computing time needed for the calculation of the electric near field for a certain height and frequency adds up to 16 h on the HP workstation. The simulations reproduce the measured data as depicted in the upper parts of Figs. 4 and 5 very accurately concerning location, extension, amplitude, and phase except for the signal peaking at $x = 0$ and $y = 15$ mm. This contribution is not accessible in the measurement due to the semi-rigid cable connected along the y axis (center of cable at $x = 0, y > 0$). The frequency offset of about 100 MHz between the calculated and the measured data results from the infinitely extended substrate assumed in the calculations.

Parasitic modes are predominantly excited in the bias gaps. Due to the orientation of the gaps, the modes in the gaps reveal no electric field in y direction and consequently are not

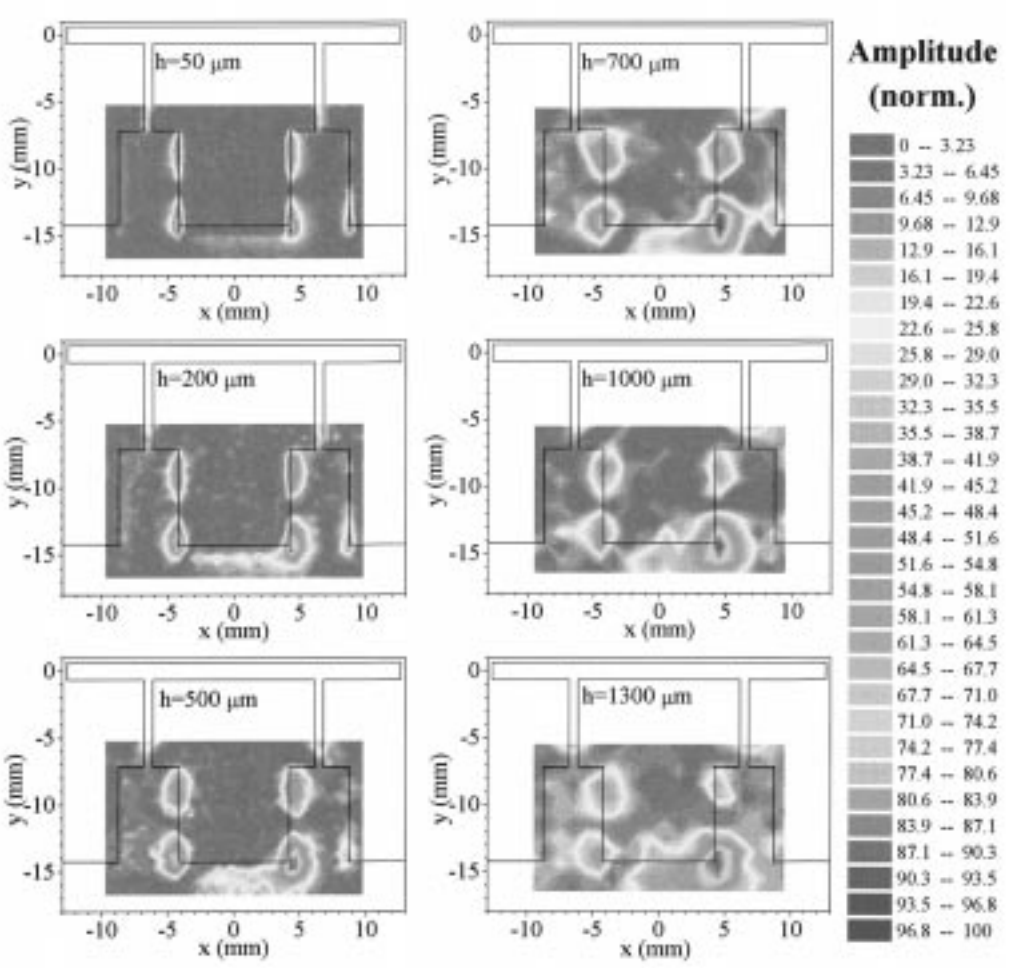

Fig. 7. Magnitude of the x component of the electric field at 6.76 GHz measured for increasing probing distances h, as indicated in the figure.

visible in Figs. 4 and 5. For sampling of the x component, the resonator is rotated by 90° relatively to the EO crystal. In Fig. 6, the amplitude of the x component of the electric field measured at 50-μm height above the bias gaps for a fixed input power of 15 dBm is depicted for driving frequencies varying from 6.1 to 6.9 GHz. The scans extend only over parts of the resonator structure (colored area), not the whole resonator. The stronger localization of the peaks in contrast to Fig. 4 is a direct consequence of the lower detection height. Maximum peak amplitudes are observed at 6.5 and at 6.76 GHz in good agreement with the S-parameter measurements. For frequencies below 6.5 and above 6.76 GHz, the electric fields appear with a significantly lower amplitude. A probable reason for the slight offset of 0.15 and 0.06 GHz between the main resonance frequencies obtained by the network analyzer and the EO measurements is that different probe stations and different clamps for adjustment of the resonator have been employed. The highest signal contributions are present at the inner T-shaped conductor and appear at fixed spatial locations independent from the operation frequency. A closer inspection reveals that the pairs of signals peaking at the (x/y) coordinates around (-4 mm/-9 mm) and (4 mm/-14 mm) at (-4 mm/-14 mm) and (4 mm/-9 mm) each are in phase but have a relative phase offset of 180°. This modal distribution clearly points to an excitation of a microstrip-like mode between the T-shaped inner conductor of the bias gaps and the backside metallization layer. The mode can be understood as a standing-wave pattern where the field is reflected between the lower end of the conductor at $y = -14$ mm and the lower edge of the bar of the T-shaped metallization at $y = -7$ mm. The tight coupling of this mode to the fundamental slot mode is evident by the fact that the amplitudes are maximal at exactly the same frequency of 6.76 GHz. When the frequency is swept through this resonance, additional signals appear at the outer metallization (e.g., at -9 mm/-14 mm), both at higher and lower frequencies. These contributions show also microstrip-like behavior and are excited by electric field coupling from the inner to the outer conductor. In addition, a co-planar slot mode is excited in the area of the narrow gaps. As a result of the dimensions of the outer metallization, the electric field distribution is asymmetric even in the gap area. This becomes obvious from Fig. 6 for the data obtained at 6.76-GHz data where stronger fields are measured at the outer metallization of the right gap compared to the left gap. The simulated data, which are not shown, are in good agreement with the calculations.

In a final experiment, we demonstrate that our technique is capable at measuring in three dimensions in order to map the

evolution of the near-field pattern with increasing height. The divergence of the emitted fields and the transition from near to far field are measured with a spatial resolution defined by the optical integration path (crystal thickness). In Fig. 7, the measured amplitude of the x component in the bias gap area is depicted for fixed frequency (6.76 GHz) and for different probing heights. The data are obtained at fixed input power, but are normalized to the peak amplitude for clarity. The fields spread out with increasing distance and, in addition, the spatial distribution becomes more asymmetric.

VI. Conclusion

In summary, we demonstrate the application of the external electro-optic sampling method for spatial mapping of electric near-field patterns on planar resonators. The technique, based on a novel femtosecond-laser synchronization scheme, covers a frequency range up to at least 150 GHz with a lateral spatial resolution as good as 10 μm. Applying this method to a recently proposed resonator design for automotive applications, we gain important information about the local behavior of the resonant structure. The field data of the investigated 7-GHz planar resonator give clear evidence for strong excitation of parasitic patch and microstrip modes not tolerable in most applications. We have shown that the electric near field can be accurately modeled with an EFIE analysis. However, the simulation is time consuming, emphasizing the advantage of the electro-optic probing technique.

Acknowledgment

The authors would like to thank V. Sommer (Institut für Halbleitertechnik I, RWTH, Aachen, Germany) for technical assistance in the S-parameter measurements.

References

[1] T. Löffler, T. Pfeifer, H. G. Roskos, and H. Kurz, *IEEE Photon. Technol. Lett.*, vol. 7, p. 1189, Oct. 1995.
[2] T. Löffler, T. Pfeifer, H. G. Roskos, H. Kurz, and D. W. van der Weide, "Stable optoelectronic detection of free-running microwave signals with 150 GHz bandwidth," in *5th Eur. Conf. Electron Opt. Beam Testing*, Wuppertal, Germany, Aug. 1995; *Microelectron. Eng.*, vol. 31, p. 397, 1996.
[3] B. H. Kolner and D. M. Bloom, *IEEE J. Quantum Electron.*, vol. QE-22, p. 79, Jan. 1986.
[4] W. Mertin, A. Leyk, G. David, R. M. Bertenburg, S. Koßlowski, F. J. Tegude, I. Wolff, D. Jüger, and E. Kubalek, in *Technol. Conf. Dig. IEEE Microwave Theory Tech.*, San Diego, CA, 1994, vol. 3, p. 1597.
[5] G. David, R. Tempel, I. Wolff, and D. Jaeger, "In-circuit electro-optic field mapping for function test and characterization of MMICS," in *Tech. Dig. IEEE Microwave Theory Tech.*, San Francisco, CA, June 1996, pp. 1533–1536.
[6] Y. Imaizumi, M. Shinagawa, and H. Ogawa, "Electric field distribution measurement of microstrip antennas and arrays using electro-optic sampling," *IEEE Trans. Microwave Theory Tech.*, vol. 43, p. 2402, Sept. 1995.
[7] T. Pfeifer, T. Löffler, H. G. Roskos, H. Kurz, M. Singer, and E. M. Biebl, "Electrooptic measurement of the electric near-field distribution of 7 GHz planar resonator," *Electron. Lett.*, vol. 32, p. 1305, 1996.
[8] T. Pfeifer, T. Löffler, R. Martini, H. G. Roskos, H. Kurz, M. Singer, and E. M. Biebl, "Spatial mapping of the near-field radiation pattern of a 7-GHz resonator," in *Tech. Dig. Conf. Lasers Electro-Optics*, Anaheim, CA, June 1996, p. 137.
[9] M. Singer, T. Pfeifer, T. Löffler, H. G. Roskos, H. Kurz, and E. M. Biebl, "Nearfield calculation of planar antennas using the electric field integral equation," in *PIERS'96*, Innsbruck, Austria, July 1996, p. 550.
[10] J.-F. Luy and P. Russer, *Silicon-Based Millimeter-Wave Devices*, W. Engl, Ed. Berlin, Germany: Springer-Verlag, 1994.
[11] A. Stiller, E. M. Biebl, J.-F. Luy, K. M. Strohm, and J. Buechler, "A monolithic integrated millimeter wave tranmitter for automotive applications," *IEEE Trans. Microwave Theory Tech.*, vol. 43, p. 1654, July 1995.
[12] Terametrics, Crofton, MD.
[13] J. A. Valdmanis, "Electro-optic measurement and techniques for picosecond materials, devices, and integrated circuits," in *Measurements of High-Speed Signals in Solid State Devices*, R. B. Marcus, Ed. San Diego, CA: Academic, 1990, p. 135.
[14] J. Son, J. V. Rudd, and J. F. Whitaker, "Noise characterization of a self-mode-locked Ti : Sapphire laser," *Opt. Lett.*, vol. 17, p. 733, 1992.
[15] W. Mertin, C. Roths, F. Taenzler, and E. Kubalek, "Probe tip invasiveness at indirect electro-optic sampling," in *Microwave Theory Tech. Soc. Conf. Dig.*, vol. 3, p. 1351, 1993.
[16] T. Itoh, "Spectral domain immitance approach for dispersion characteristics of generalized printed transmission lines," *IEEE Trans. Microwave Theory Tech.*, vol. MTT-28, p. 733, July 1980.

Torsten Pfeifer was born in Kamen, Germany, in 1967. He received the Dip. degree in physics, in 1993, and the Dr.Ing. degree in electrical engineering, in 1997, both from the RW Technische Hochschule (RWTH), Aachen, Germany.

He is currently with the Daimler-Benz Aerospace (DASA) in Ülm, Germany. His research interests include the development and application of high-speed opto-electronic techniques for the characterization of ultrafast electric and opto-electronic devices and circuits.

Torsten Löffler was born in Winterberg, Germany, in 1970. He received the Dip. degree in physics from the RW Technische Hochschule (RWTH), Aachen, Germany, in 1996.

His research interests include the synchronization of free-running lasers to millimeter-wave sources and the application of high-speed opto-electronic techniques.

Hartmut G. Roskos was born in Freiburg, Germany, in 1959. He received the Dip. and Ph.D. degrees from the Technical University (Karlsruhe and Munich, Germany), in 1985 and 1989, respectively, and the Habilitation degree in physics from the Institut für Halbleitertechnik II of the RW Technische Hochschule (RWTH), Aachen, Germany, in 1996.

From 1989 to 1991, he worked at AT&T Bell Laboratories, Holmdel, NJ, as a Postdoctoral Fellow, pursuing research in the fields of ultrafast opto-electronics and time-resolved terahertz spectroscopy. From 1991 to 1996 he was with the RWTH, Aachen, Germany. Since 1997 he has been a Full Professor of physics at the Johann Wolfgang Goethe-Universität, Frankfurt am Main, Germany. His main research activities focus on spectoscopy of ultrafast phenomena in semiconductors and superconductors in the optical and terahertz frequency ranges and on high-speed device development and characterization.

Heinrich Kurz was born in Pennewang, Austria, He received the Ph.D. degree in experimental physics from the University of Vienna, Austria, in 1971.

He was with the Philips Research Laboratories, Hamburg, Germany, from 1971 to 1981. From 1981 to 1984 he was with Harvard University, Cambridge, MA. Since 1984 he has been a Professor of electrical engineering at the RW Technische Hochschule (RWTH), Aachen, Germany. Recently, he founded an extra-university Center for Applied Micro- and Opto-electronics (AMO GmbH). His current interests include ultrafast solid-state phenomena, application of femtosecond laser technology, high-speed device characterization, Si-based nanostructures, and novel materials for micro-electronics such as SiC and high-T_c superconductors.

Markus Singer was born in Rosenheim, Germany, in 1966. He received the Dipl.Ing. and the Dr.Ing. degrees from the Technical University, Munich, Germany, in 1993 and 1997, respectively.

From 1993 to 1997, he was a Research Associate at the Lehrstuhl für Hochfrequenztechnik of the Technical University, Munich. Since 1997 he has been with Daimler-Benz Aerospace, Military Aircraft Division, as a System Engineer. His research interests include field-theoretical analysis of planar antennas and resonators and silicon-based integrated millimeter-wave devices.

Erwin M. Biebl was born in Munich, Germany, in 1959. He received the Dipl.Ing., Dr.Ing, and the Habilitation degrees from the Technical University, Munich, Germany, in 1986, 1990, and 1993, respectively.

In 1986, he joined Rohde & Schwarz, Munich, where he was involved in the development of mobile radio communication test sets. Since 1988 he has been with the Institut für Hochfrequenztechnik of the Technical University, Munich, where he is now University Lecturer and Head of the millimeterwave devices group. His research interests include optical communications and integrated optics, field-theoretical analysis of planar resonators and antennas, quasi-optical measurement techniques, and design and characterization of integrated millimeter wave devices.

Dr. Biebl was the recipient of the Dr. Georg Spinner Award in 1991. In 1996 he was co-recipient of the Informationstechnische Gesellschaft (ITG) Award. He is a member of the ITG in the Verband Deutscher Elektrotechniker (VDE), Germany.